JOURNAL OF MECHANICAL ENGINEERING AND SCIENCES
ISSN: 2289-4659 e-ISSN: 2231-8380
VOLUME 19, ISSUE 2, 2025, 10577 - 10594
DOI: https://doi.org/10.15282/jmes.19.2.2025.1.0829

RESEARCH ARTICLE

Optimized design and performance analysis of a high-pressure radial turbine for energy recovery applications

N. S. Ahmad[1], M. N. Azman[1], A. M. I. Bin Mamat[1,2]*

[1] College of Engineering, Universiti Teknologi MARA, 40450, Shah Alam, Selangor Darul Ehsan, Malaysia
[2] Smart Manufacturing Research Institute (SMRI), Universiti Teknologi MARA, 40450, Shah Alam, Selangor Darul Ehsan, Malaysia
Phone: +6035543 5251; Fax.: +6015543 5052

ABSTRACT - Single-cylinder direct-injection engines suffer significant exhaust energy losses, but designing efficient radial turbines for such systems requires physical characterization of pulsating flows and thermal stresses. This paper investigates the design and performance of a 500W high-pressure radial turbine of waste energy recovery for a single-cylinder engine. The main objective of this study is to optimize the turbine's dimensions and efficiency for capturing exhaust energy upstream of catalytic converters in internal combustion engines. Employing a two-stage computational approach, numerical modeling first established key geometric parameters including a 19.3 mm inlet radius, 5.1 mm leading-edge length, 72° inlet angle, and 0.7 outlet radius ratio,followed by CFD simulations in ANSYS CFX using a 212,212-element single-passage mesh at 50,000, 70,000 rpm and 90,000 rpm, and 800 K inlet temperature. The optimized turbine demonstrated peak efficiency of 67% at 0.005 kg/s mass flow rate, revealing that systematic numerical optimization significantly enhances energy conversion efficiency. These results provide critical insights for developing compact, high-efficiency turbines for exhaust energy recovery systems, advancing waste heat utilization technology.

ARTICLE HISTORY
Received : 11th Sept. 2024
Revised : 06th May 2025
Accepted : 10th June 2025
Published : 30th June 2025

KEYWORDS
Turbomachinery
Radial turbine
Numerical analysis
CFD analysis

1. INTRODUCTION

The internal combustion engine produces greenhouse gases (GHGs) from the combustion process. The application of biofuels can reduce these harmful GHGs [1]. Despite only decreasing the GHGs, biofuels could not increase engine performance. Increasing the air intake pressure will increase the engine performance and increase the power output [2]. The supercharging system can increase the air intake pressure, which uses either the supercharging or turbocharging system. The turbocharging system utilises the exhaust energy of a radial turbine to drive the compressor impeller, which is used to compress and increase the intake pressure [3]. The study of turbocharging system and the radial turbines in internal combustion engines has gained significant traction due to their potential to enhance engine performance by improving efficiency and power output [4]. The turbocharging system operates by increasing the amount of air entering the combustion chamber, which in turn boosts the power of the internal combustion engine. This mechanism is particularly effective because the centrifugal compressor, one of the main components of a turbocharging system, is powered by the kinetic energy of exhaust gases, which would otherwise be wasted [3]. This energy is harnessed to increase the density of the intake air, allowing a greater mass of air to enter the combustion chamber, thus improving the engine's overall fuel efficiency [5].

The radial turbines, which are crucial components of turbochargers, have been extensively studied for their efficiency in energy transfer in various applications, including turbochargers, small power plants, and aircraft engines. The fundamental design of radial turbines involves the fluid entering axially and then being guided radially through a set of blades, which leads to the rotation of the impeller and the generation of mechanical energy [6]. The main problem in the current radial turbine design is to obtain suitable design parameters that meet the operating requirements. Generally, commercial turbomachinery design software lacks the performance analysis to help the designer make decisions. Integrating computational fluid dynamics into the turbomachinery design will assist the design process and reduce the design timeframe. The optimization of these parameters is essential for enhancing their performance and efficiency, and the process requires careful evaluation of their dimensions, geometry, and other parameters during the design phase [7]. The volute of the radial turbine is correlated with the Area Ratio, A/R of the volute and turbine design [8, 9]. The geometric configuration of the turbine can be generated by using Bezier curve method [10].

The turbomachinery design process is inherently complex, often beginning with defining initial design requirements and progressing through phases that involve modifying geometric parameters with parametric variations [11]. This is typically followed by simple calculations under the assumption of steady and one-dimensional flow, which allows for investigating a limited set of design options [12]. However, as highlighted by Noughabi and Sammak [13], a more detailed design and analysis approach is necessary for radial turbines, which generally involves defining the turbine's geometry and making state assumptions on losses to calculate efficiency. This procedure helps estimate key performance

*CORRESPONDING AUTHOR | A. M. I. Bin Mamat | ✉ amanihsan@uitm.edu.my

parameters, such as expansion ratio, mass flow rate, power output, and efficiency, producing a performance map for the turbomachinery design. The performance map is a characteristic of the designed turbomachinery and can be scaled up or down according to the requirements [14].

One critical aspect of improving radial turbine design is Computational Fluid Dynamics (CFD). This tool has become indispensable in fluid mechanics for predicting mass and heat transfer, fluid movement, and related phenomena. The analysis can be used to improve the turbomachinery design. CFD allows for the analysis and resolution of fluid flow issues with high accuracy. However, the effectiveness of CFD models heavily depends on their precision, and there are inherent limitations, such as the simplifications made to reduce computational demands [15]. Despite the advantages of CFD, traditional methods such as Reynolds-Averaged Navier-Stokes (RANS) and Unsteady Reynolds-Averaged Navier-Stokes (URANS) have limitations, particularly in heat transport and turbulence modelling [16]. These limitations often necessitate simplifications of geometric and operating conditions, which can affect the accuracy of the simulations. However, CFD remains a powerful tool for understanding the internal flow behaviour within turbomachines and for designing and producing efficient machines for various industrial applications. A single passage analysis for the radial turbine can minimise the computational time and efficiently analyse the internal flow in the radial turbine [17]. Structural strength requirements limit radial turbine aerodynamics by restricting blade speed and pressure ratios. However, mixed-flow designs with non-radial fibre orientation reduce centrifugal stress, enabling higher performance without material advances [17].

Several studies have demonstrated the application of CFD in turbomachinery analysis. For instance, Borovkov et al. [18] employed CFD simulations to predict the aerodynamic performance of a low-speed impeller, while Yu et al. [19] used CFD to investigate the aerothermodynamics performance of the turbomachinery design for a turbocharging system in an internal combustion engine. These studies underline the importance of CFD in optimizing turbomachinery components, particularly in scenarios where traditional experimental methods may be impractical or too costly. The use of CFD in analysing high-pressure turbines, particularly in off-design conditions, is also noteworthy. High-fidelity CFD modelling of such turbines is challenging due to the complex blade designs [20]. Nonetheless, CFD allows for examining the relationship between flow behaviour and turbine performance under various operating conditions, making it a critical tool for optimizing turbine design [21]. Bin Mamat et al. [12] al used the flow field analysis in the ANSYS CFX to optimise the Low-Pressure Turbine design point. The flow field analysis in a single passage CFD analysis was used to optimise the inlet absolute angle, α_1 at the design point.

In summary, the literature emphasizes the critical role of turbochargers and radial turbines in enhancing the performance of internal combustion engines. While traditional design methods and one-dimensional analyses provide a foundational understanding, integrating CFD in the design and analysis process offers a more detailed and accurate approach to optimizing these components. The continued advancement of CFD techniques and their application in turbomachinery design is essential for further improving the efficiency and performance of these systems. The main objective of this paper is to present a comprehensive method to design a low-energy radial turbine by integrating the one-dimensional turbine modelling with the CFD technique. The first part presents a numerical one-dimensional rotor design that implements theoretical equations from turbomachinery, fluid mechanics, and thermodynamics. Thereafter, the turbine rotor design was constructed in a three-dimensional virtual design. Finally, Ansys CFX was used to evaluate the turbine off-design operating performance.

2. MATERIALS AND METHODS

2.1 Numerical Rotor Design

The radial turbine rotor transfers energy from the hot gas, and the design process typically starts from the Euler turbomachinery equation. This study employed a systematic method to establish the basic design. The approach accelerated progress toward the ultimate objective by implementing a starting point design, streamlining the overall design and optimization process. Figure 1 depicts a typical turbine rotor. The rotor blades are typically radial at the inlet, as this configuration optimises stress conditions. Early design procedures for achieving the best efficiency point assumed that the inlet relative velocity vector aligned with the radial blade, resulting in a right-angled velocity triangle. However, experimental data and incidence loss models have shown that a significant angle of incidence occurs at the best efficiency point, making the velocity triangle more accurate.

At the inlet, it is assumed that the blades were radial. It was discovered that the best efficiency occurred when the flow at the inlet did not exactly match the blade but at some negative incidence. The mismatch is due to the blade loading creating a huge static pressure gradient across each passage, pushing the flow from the pressure to the suction surface in the opposite direction of rotation. As a result, the incidence angle at which the best efficiency occurred had to be determined. The incidence angle of a rotor with radial blades coincides with the angle of approach of the relative velocity vector, β_1 [11] At the design stage, the fluid is usually believed to be discharged from the rotor in an axial direction. By integrating this Equation with the velocity triangles at the inlet and outlet, an expression for work transfer per unit mass flow based on fluid and rotor velocities is derived. In such cases, the Euler turbomachinery equation looks like this:

$$\frac{\dot{W}_T}{\dot{m}} = U_1 C_{\theta 1} - U_2 C_{\theta 2} = h_{01} - h_{02} \tag{1}$$

$$\frac{\dot{W}_T}{\dot{m}} = \frac{1}{2}[(U_1^2 - U_2^2) - (W_1^2 - W_2^2) + (C_1^2 - C_2^2)] \quad (2)$$

Subscripts 1 and 2 correspond to the rotor inlet and exit planes.

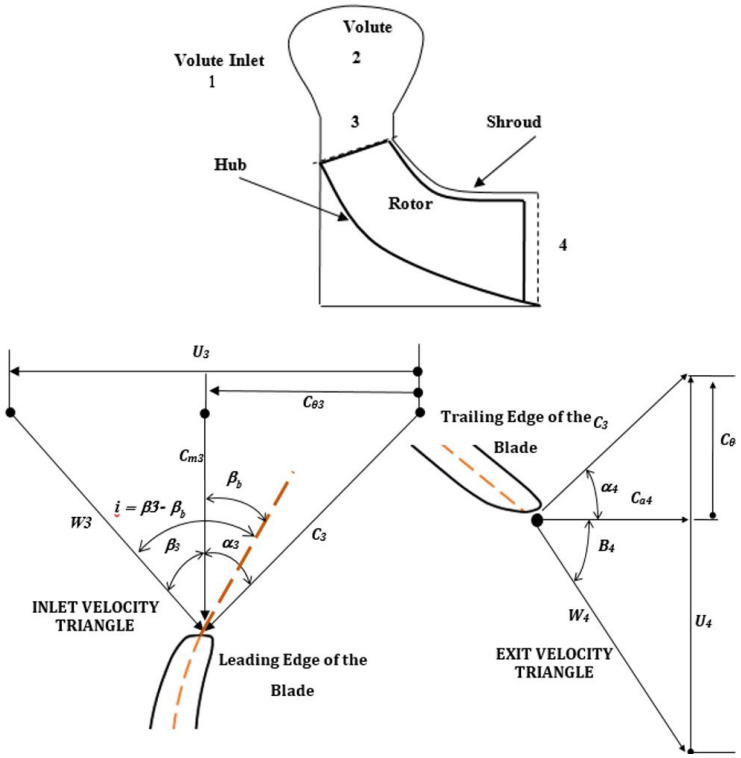

Figure 1. Velocity triangle of a turbine rotor

The objective is to maintain flow velocities as low as possible since various losses, such as friction and exit kinetic energy, increase with the square of velocity. While optimising for high efficiency would focus primarily on energy utilisation, achieving high specific work production is often equally or more important. This scenario necessitates a compromise, as it anticipates higher velocities in particular areas of the machine. The typical configuration of the velocity triangles at the rotor's inlet and outlet aims to enhance relative velocity while reducing absolute velocity through the rotor [22]. The magnitude of rotation and relative velocity are highest at the tip. By setting $C_{\theta 1}$ equal to U_1 and $C_{\theta 2}$ equal to 0, the energy equation is simplified when the inlet flow angle relative to the blade is zero, and the absolute exit velocity is axial.

$$\frac{\dot{W}_T}{\dot{m}} = U_1^2 \quad (3)$$

The blade speed directly influences the specific work output. Designers typically adhere to a maximum value for U_1, which is determined by factors such as the rotor material and the turbine's operating temperature. Follows that:

$$\left(\frac{U_1}{a_{01}}\right)\left(\frac{C_{\theta 1}}{a_{01}}\right) = \left(\frac{S_w}{\gamma - 1}\right) \quad (4)$$

The number of turbine blades is given by the empirical correlation from Whitfield and Baines [11], which is given in Eq. (5):

$$Z_B = \frac{\pi}{30}(110 - \alpha_2)\tan\alpha_2 \quad (5)$$

The enthalpy-entropy, *h-s* diagram in Figure 2 represents thermodynamic processes in a radial turbine rotor. The Figure shows how energy is transferred or lost during the turbine's operation. Changes in temperature and entropy of the working fluid are illustrated as it passes through the different stages of the turbine. At the initial stage, the fluid flows into the turbine. Changes occur as the fluid moves through the turbine, as state points 1, 2, 3, and 4 illustrate. These points represent crucial moments in the flow development throughout the turbine volute (1 – 2), stator (2 -3) and rotor (3 – 4). In the ideal case where entropy remains constant, it is called isentropic processes, such as 1 – 3 and 3 – 4 on the h-s diagram, indicating an isentropic fluid expansion through the turbine as a subscript of is. However, in the actual process, there are losses due to friction, turbulence, and other heat losses and thus entropy increases illustrated by the curved lines from 1 to 3 and 3 to 4 [7], [23]. The *h-s* diagram is useful for determining the rotor design, cooling systems, and working conditions of the radial turbines. Through entropy changes and temperature drops, optimisation and modifications can be made to reduce losses and maximise efficiency.

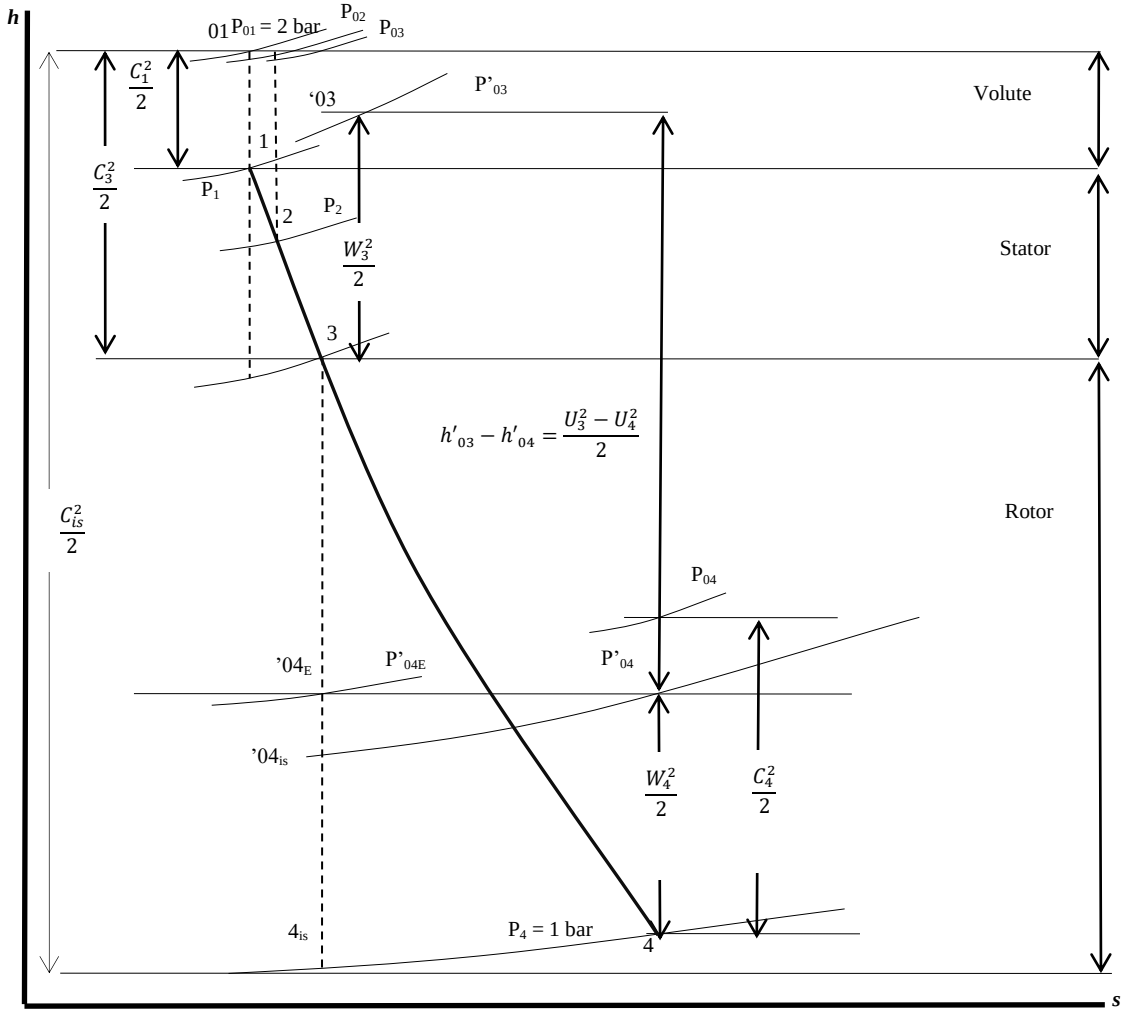

Figure 2. Enthalpy-entropy diagram

2.1.1 Rotor Design Parameters

The rotor design process is fundamental to ensure the turbine's performance and efficiency. This section discusses and presents the key design parameters obtained from the preliminary analysis. The inlet conditions of the turbine were crucial for establishing the numerical analysis of the radial turbine. The inlet conditions included the mass flow rate, pressure ratio, total pressure, inlet temperature, and power output. The operating conditions for the radial turbine are given in Table 1, where the variables will be used to derive the turbine's key parameters. In the initial stage of designing a radial turbine, key parameters such as the Mass Flow Parameters, *MFP*, Pressure Ratio, *PR*, Specific Speed, *SP* and Total-to-static Efficiency, $\eta_{T\text{-}s}$ must be assumed or specified to guide the design process. These parameters help define the turbine's operation and performance [11, 24].

Table 1. Turbine design parameters

Items	Specifications
Mass flow rate, $\dot{m}$ (kg/s)	0.025
Rotation speed, N (rpm)	70 000
Power output (W)	500
Pressure ratio, PR	2
Inlet temperature (K)	800
Inlet Pressure (kPa)	200

2.2 Three-Dimensional Modelling

Three-dimensional (3D) modelling of radial turbines is a complex process of creating representations of turbine components using computer-aided design (CAD) in detail and accuracy. It is important to analyse and optimise the turbine's performance and prototype it under various operating conditions. The process of 3D modelling starts with a conceptual design phase where the general geometry of the turbine and key parameters such as blade size, rotor and casing

are defined. CAD software can create accurate 3D models of each component, like complex curves and surfaces of the turbine blades, using CATIA, SolidWorks or Autodesk Inventor. Blade geometry generation, angles, and thicknesses were computed and generated using Bezier Polynomials. Tools such as MS Excel were used to develop the algorithm, and the profiles were initially visualized.

Bezier polynomials are mathematical algorithms that help to create smooth curves for many applications, from computer graphics to animation and industrial design to blades. A Bezier polynomial is a formula showing a curve controlled by a series of control points. The curve does not pass through all the control points but is influenced by them, thus making a smooth design. A fourth-order Bezier polynomial is defined with five control points, which are P_0, P_1, P_2, P_3, *and* P_4. In this study, the Bezier curve of fourth order was used to generate the meridional and camberline curvature, which is given by Eq. (5).

$$B(u) = (1-u)^4 p_0 + 4(1-u)^3 u p_1 + 6(1-u)^2 u^2 p_2 + 4(1-u)u^3 p_3 + u^4 p_4 \quad (5)$$

where u ranges between 0 and 1, each of the terms in this Equation forms a point on the curve, while the coefficients become the binomial coefficients that ensure that the curve passes through the given points of control. Bezier polynomials are very important in design because they can produce smooth, continuous curves with easy adjustments by control points. Thus, it is suitable for application in modelling complex shapes and surfaces. Bezier polynomials specify the blades' meridional sections for the camber line. The camber line describes the mean line of curvature of a blade. Using Bezier curves, one can create a blade profile and fine-tune the curvature for desired aerodynamic properties.

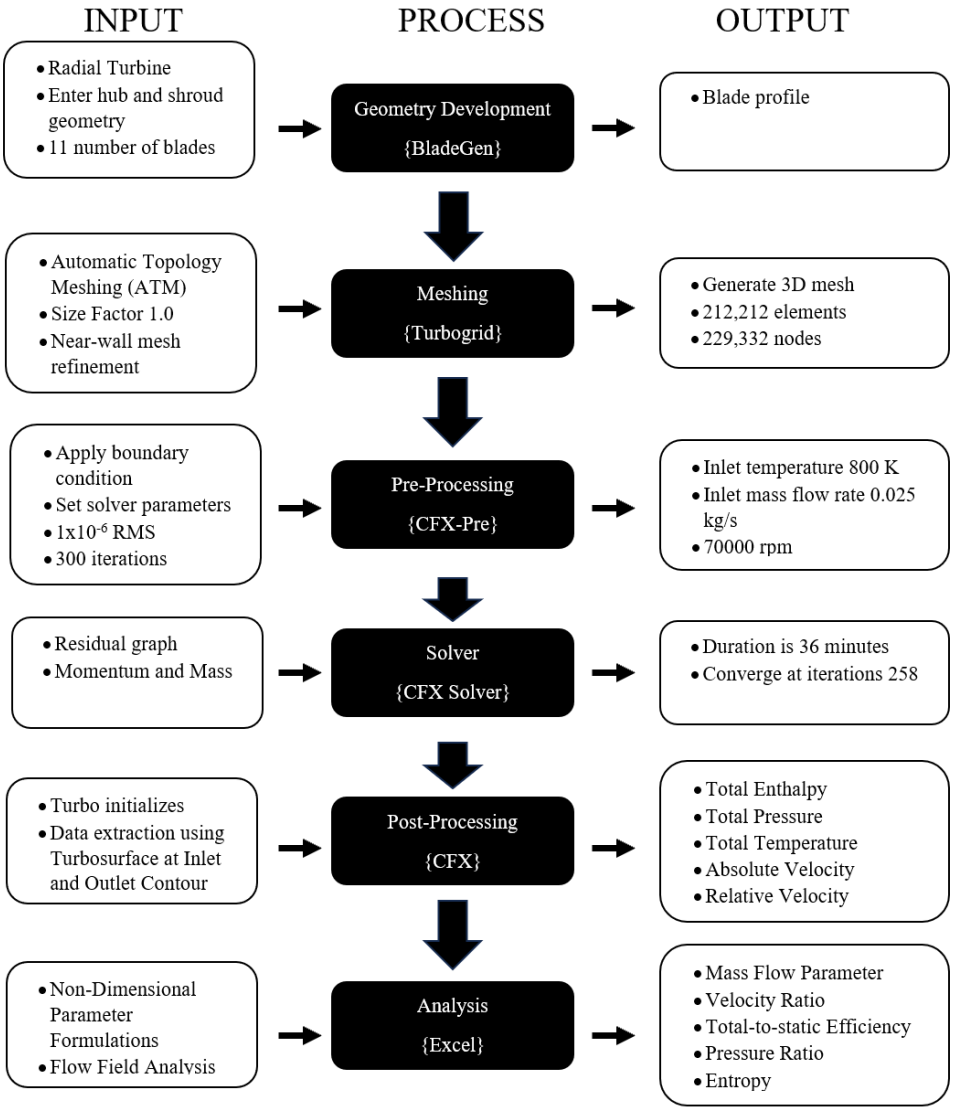

Figure 3. Flow Chart of the CFD Procedures in Ansys CFXs

2.3 Computational Turbine Performance Set Up

The purpose of computational analysis is to simulate and analyse the performance and flow field pattern around the high-pressure turbine by using Computational Fluid Dynamics (CFD) software as a tool. There are a few processes that are required to evaluate high-pressure turbine, which are Geometry Generation (Bladgen CFX), Mesh Generation (Turbogrid), Pre-Processing (Pre-CFX), Solver (ANSYS CFX), Post-processing and then continue with Data Extraction

where all the data will be obtained. Figure 3 shows the flow chart for the procedures in the Ansys CFX for the CFD analysis. The governing equations for fluid flow are derived from the fundamental principles of mass conservation, momentum conservation, and energy conservation, which are known as the RANS equations for the turbulent flow model in the CFD analysis. The Eddy Viscosity Models (EVM) was used to model the turbulence flow model in the radial turbine.

2.3.1 Geometry Generation (BLADEGEN CFX)

The turbine impeller's blade profile will be created in the first stage, utilising ANSYS BladeGen as the modeller and the design requirement measurement. As illustrated in Figure 4(a), the hub and shroud geometry of the blade profile will be input into the meridional form coordinates. At the inlet, the hub radius, r_{1h}, was set up at Z = 0. Moving horizontally along the shroud, the radius remains constant at Z, to create a leading edge (LE) section. Progressing down the curved section, the shroud radius, r_{1s}, decreases, with significant points at Z, where the radius transitions to create the trailing edge (TE). The blade thickness is fixed to 1 mm.

Furthermore, 10 to 11 blades were incorporated into the total rotor design. These variables are essential for delineating the blade's principal geometrical characteristics. As Figure 4(b) demonstrates, a blade-to-blade graphical user interface is used to visualise and fine-tune the blade shape for the camberline, pressure surface, and suction surface curvature.

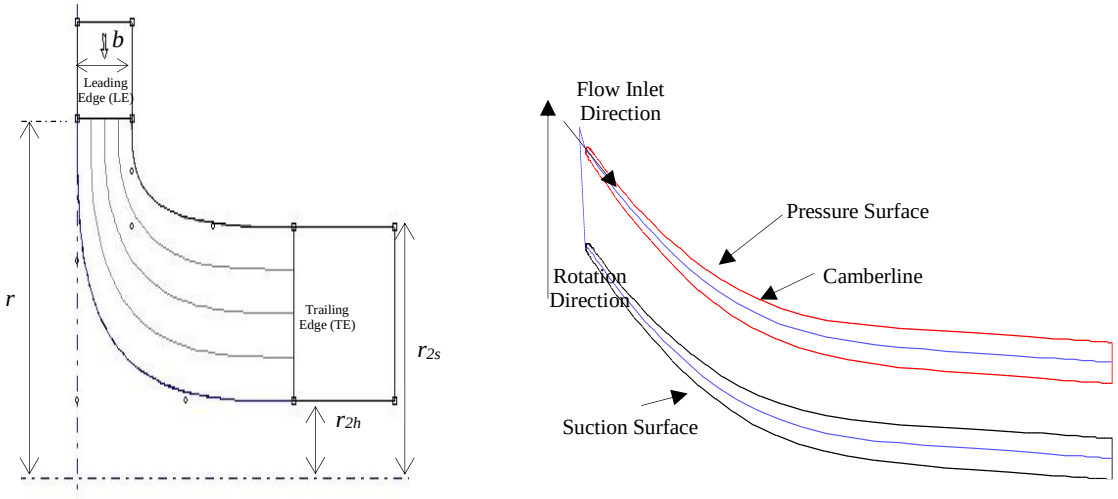

(a) (b)

Figure 4. (a) Meridional view and (b) Blade-to-blade the generated camberline

2.3.2 Mesh Generation

Meshing, the technique of splitting the computational domain into discrete, small pieces called cells, is crucial to Computational Fluid Dynamics (CFD) simulations. The mesh's quality directly impacts the accuracy and effectiveness of the simulation. To produce correct results, a good mesh should have the right element size, aspect ratio, skewness, and orthogonality. It has capabilities like automated refinement, structured meshing for turbomachinery components, and even hybrid meshing for complex geometries. ANSYS TurboGrid was used in the meshing process to create a mesh with 212,212 elements and 229,332 nodes for the high-pressure turbine component. Figure 5 shows the single passage meshing elements generated using TurboGrid. The meshing parameters are related to a turbine blade's computational fluid dynamics (CFD) aerodynamic modelling. This single-passage method is similar to Fattah et al. [17].

The Advancing Front Method (ATM) in the Topology Mesh Technique is a progressive and adaptive meshing procedure that manages complex geometries well. When the Size Factor value is set at 1, the original mesh size should be used as the baseline. The application of the Boundary Layers Refinement Control function, which is based on mesh size, suggests using a finer mesh in the vicinity of the boundary layers to capture intricate flow features and improve accuracy in crucial areas. Due to its proportionality, the Spanwise Blade Distribution Parameter generated constant resolution by adjusting the mesh distribution along the blade's span by the blade's geometry. To maintain mesh quality and accuracy in simulations, the Hub Tip Mesh Method, which matches expansion at the blade tip, was selected to ensure the mesh grows smoothly and consistently from the hub to the tip. The meshing set-up parameters are given in Table 3.

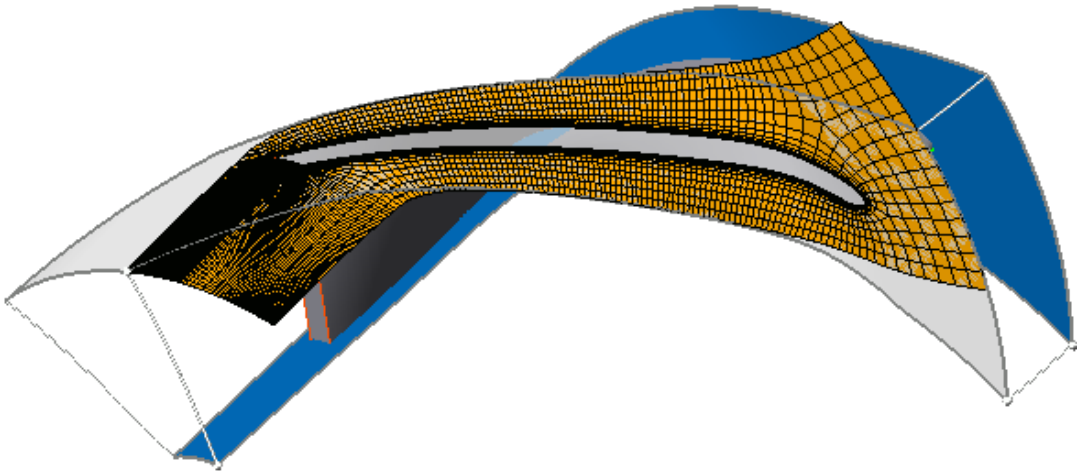

Figure 5. Meshing of single passage

Table 2. Meshing set-up parameters

Parameter	Method
Topology Mesh Technique	ATM
Size Factor	1
Boundary Layers Refinement Control	Proportional To Mesh Size
Spanwise Blade Distribution Parameter	Proportional
Hub Tip Mesh Method	Match Expansion at Blade Tip
Near Wall Treatment	Absolute

2.3.3 Pre-Processing

The preprocessing is setting up the model and simulation environment before conducting the analysis. This involves importing or producing the geometry, giving material attributes, and breaking the geometry up into finite elements to create a mesh. Table 3 depicts the solver set-up in the pre-processing for the Ansys's CFX. The fluid is described as air and is modelled as an ideal gas during the preprocessing stage of an ANSYS simulation. This simplifies the fluid's behaviour by assuming a linear relationship between pressure, volume, and temperature. The baseline pressure for the simulation is the reference pressure, which is set at 101325 Pa, or standard atmospheric pressure. The Total Energy technique represents heat transmission, guaranteeing that the simulation considers all types of energy, including kinetic and thermal energy. The selected turbulence model is k-Epsilon, a widely used turbulence model for predicting turbulence flow in the CFD simulation [25]. The k-Epsilon turbulence model balances accuracy and computational efficiency for various flow conditions. The Model solves two transport equations for the turbulent kinetic energy (k) and its dissipation rate (epsilon). This configuration guarantees a thorough and precise depiction of heat transfer and fluid dynamics inside the system under study. The Ansys CFX uses the finite Volume Method (FVM) to discretize the k-ε turbulence.

Table 3. Solver set-up

Parameter	Method
Fluid	Air Ideal Gas
Reference Pressure	101325 Pa
Heat Transfer	Total Energy
Turbulence Model	k-Epsilon

Important sections of the turbomachinery model for simulation are defined by the "Region Information" settings in Turbo Mode within ANSYS. The inner and outer boundaries where the blades are joined and encased are denoted by the terms "Hub" and "Shroud". The actual blades are specified in the "Blade" area. The "Inlet" and "Outlet" limits show where the fluid enters and leaves the domain. Assuming that the machinery repeats around the circumference, "Periodic 1" and "Periodic 2" define periodic boundaries for modelling a section of the machinery. The absence of matching between "Symmetry," "Tip 1," and "Tip 2" suggests that no particular symmetry planes or tip clearances are used in this configuration. Table 4 shows the boundary conditions set-up at the inlet and outlet of the fluid passage for the radial turbine. The thermal condition of the fluid entering the system is defined by the total temperature (T-Total), which is 800 K in the preprocessing configuration for the ANSYS simulation. The mass flow rate is applied to specific geometric passages or sections since the mass flow parameter is specified per passage. With a mass flow rate of 2.3 g/s, the fluid entering each route each second is precisely specified at the passage's inlet and outlet, as shown in Figure 6. By defining the flow direction as normal to the boundary (refer to Figure 6), which means that the fluid enters perpendicular to the

designated boundary surfaces, the boundary condition is made simpler, and the simulation's accuracy is increased by guaranteeing a consistent entry flow. In order to effectively describe the fluid dynamics and thermal characteristics inside the system, the thermal and flow parameters must be specified in detail.

Table 4. Boundary conditions set-up

Parameter	Method
T-Total	800 K
Mass Flow	Per Passage
Mass Flow Rate	0.5 2.3 $g.s^{-1}$to 10 $g.s^{-1}$
Flow Direction	Normal To Boundary
Mass Flow Parameter, MFP	0.0005 – 0.012
Pressure Ratio, PR	1.1 – 1.6
Velocity Ratio, U_2/C_{is}	0.05 – 0.65
Rotational Speed, RPM	50 000; 70 000 & 90 000

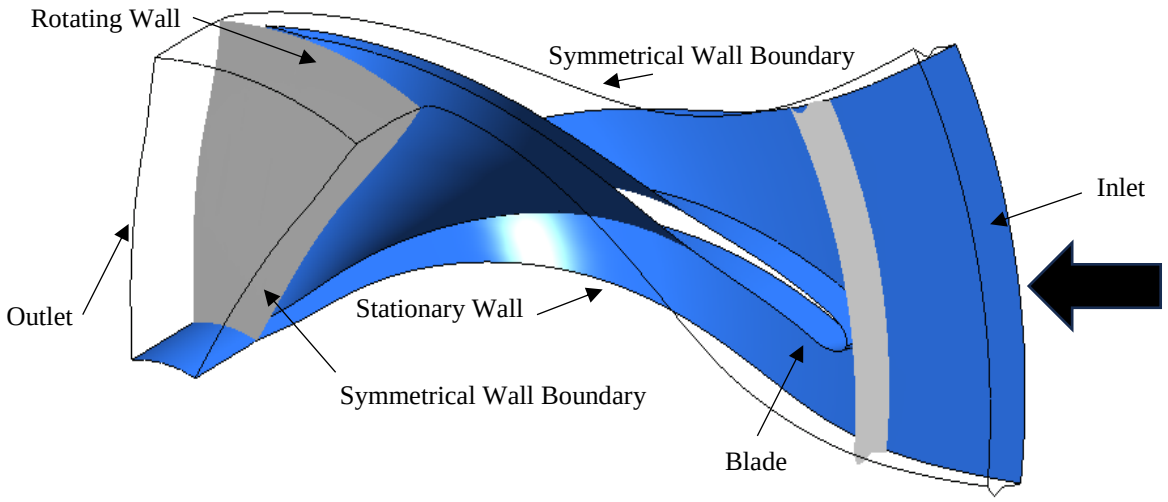

Figure 6. Boundary conditions set-up

3. RESULTS AND DISCUSSION

3.1 Rotor Geometrical Design

Figure 7 represents the relationship between the inlet length and absolute angle. As the α_1 increases from 70° to 80°, inlet length, *b* increases from 0.005 m to 0.009 m. A larger inlet angle requires a longer length, likely due to aerodynamic or structural design requirements to maintain efficient fluid flow into the turbine. Understanding this relationship is crucial for optimising turbine design, as it helps balance the desired inlet angle with the physical constraints of the inlet length to enhance overall performance and efficiency. The design specification of α_1 is 72° with an inlet length *b* of 0.005 m, which is selected due to its optimal balance between the inlet angle and the length required for effective flow. As the inlet absolute angle increases, it improves the alignment of the flow entering the turbine, reducing flow separation and enhancing the aerodynamic efficiency. The flow alignment ensures that the inlet length is sufficient to accommodate the angle, leading to smoother flow transition and minimised losses at the inlet. Optimising inlet angles reduces flow separation and enhances turbine efficiency [5]. Increased inlet length with angle helps manage flow distribution and minimises secondary flow losses, improving performance [26].

Figure 8 illustrates the correlation between the inlet absolute Mach number, M_1 and inlet absolute angle, α_1, for the specified radial turbine design. Figure 8 presents that the M_1 is decreased as the α_1 increases. As the angles of the inlet further increase, the bulk airflow that enters the radial turbine, known as meridional velocity, C_{m1}, is lower, resulting in lower Mach numbers. The value of α_1 is 72° with M_1 is 0.267, which is selected as a design parameter. A higher Mach number can lead to shock waves and higher losses, while a lower Mach number may not generate sufficient energy for the turbine. Varying the inlet angle influences the Mach number, pressure, and velocity profiles entering the rotor. Lower Mach numbers at higher angles help reduce shock losses, enhancing turbine efficiency.

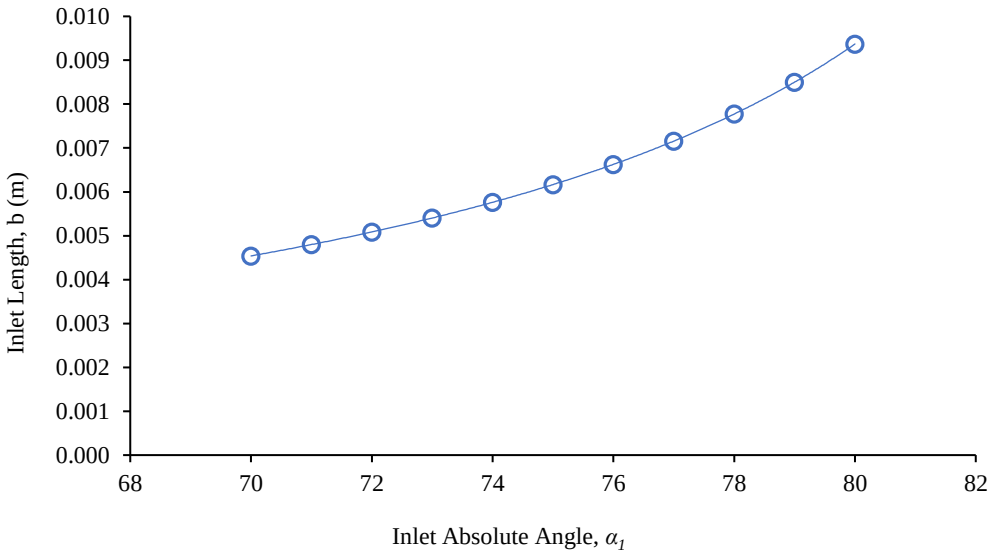

Figure 7. Inlet length at various inlet absolute angle

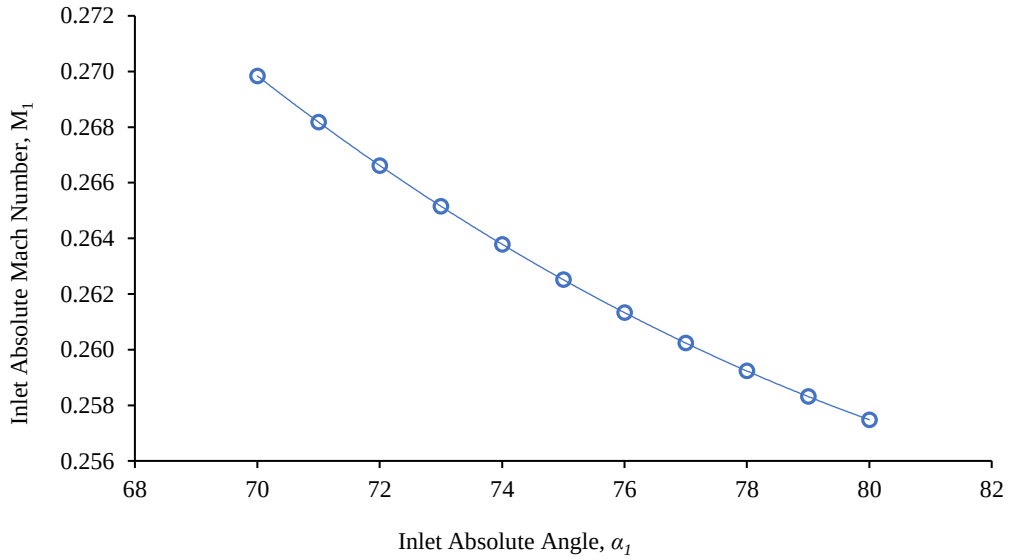

Figure 8. Inlet absolute Mach number at various inlet absolute angle

The effect of the exit relative angle, $\beta_{2,}$ is shown in Figure 9 where it is shown a significant decrease of β_2 as the outlet radius ratio, $r_{2,h}/r_{2,s}$, increases. A higher value of β_2 and $r_{2,h}/r_{2,s}$ will increase the relative velocity and decrease the height of the rotor at the exit, respectively. Also, the figure depicts the effect of the ratio of the exit radius shroud to the inlet radius, $r_{2,s}/r_1$. The value of $r_{2,s}/r_1$ must be less than 1.0. Figure 9 also depicts that the β_2 increases as the $r_{2,s}/r_1$ increases. The highlighted value β_2 of -61° when $r_{2,h}/r_{2,s}$ is 0.7 represents the chosen design parameter, optimising the relative angle for efficient exit flow conditions. This design aims for favourable exit flow conditions with minimised flow separation and aerodynamic losses. In the design point selection, it is important to optimise the exit angle to control swirl velocity and improve the alignment of exit flow with downstream components. Reducing the exit angle achieves a smoother flow transition, reducing losses and enhancing efficiency [27].

Figure 10 shows that the exit absolute Mach number, M_2, is increased as the $r_{2,h}/r_{2,s}$, is increased and the $r_{2,s}/r_1$ is decreased. At $r_{2,h}/r_{2,s}$ equals 0.7 and $r_{2,s}/r_1$ equals 0.7, and the value M_2 is 0.1. It can be seen that the absolute velocity is decreased at the exit of the turbine rotor. A lower M_2 will contribute to a larger operation ratio for the turbine rotor. Optimising the exit Mach number is important to ensure efficient turbine operation without excessive shock losses or flow distortions. Higher exit Mach numbers improve the turbine's expansion process but must be managed to avoid adverse performance effects [28].

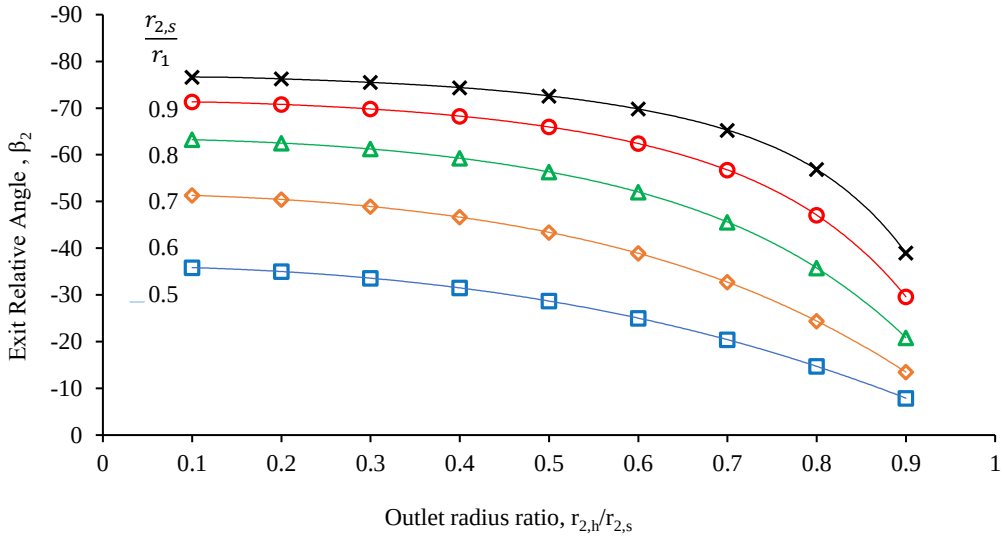

Figure 9. Exit relative angle at various $r_{2,h}/r_{2,s}$

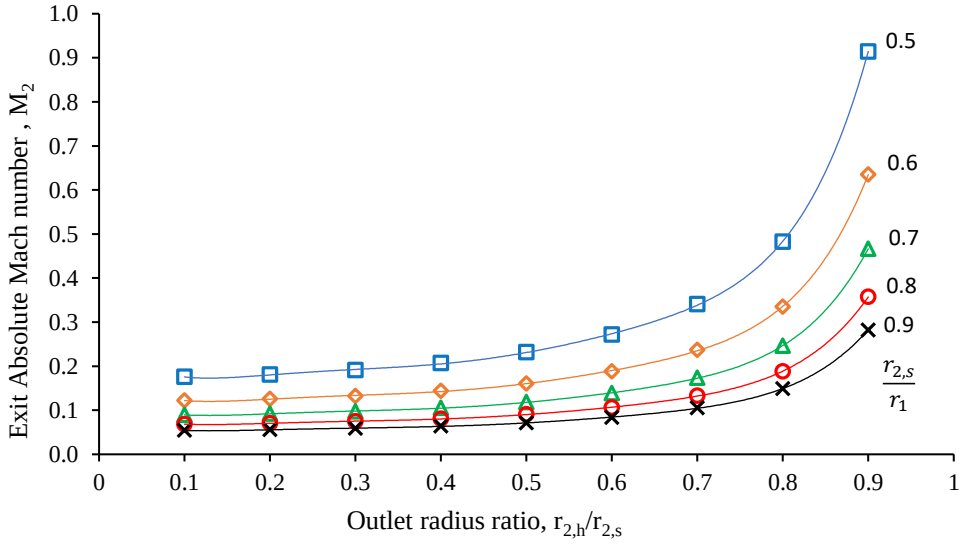

Figure 10. Exit Absolute Mach number, M_2 at various $r_{2,h}/r_{2,s}$

Figure 11 shows that the exit relative Mach number, M'_2, varies with design parameters of $r_{2,h}/r_{2,s}$, showing an increasing proportion to exit relative Mach number. Also, the M'_2 is increased as the $r_{2,s}/r_1$ is increased. The value of M'_2 is 0.2 for $r_{2,h}/r_{2,s}$ of 0.7 represents the chosen design parameter. The selected value influences the relative flow speed at the turbine exit. Despite a large relative angle, β_2, the relative velocity is low at the rotor exit. This exit condition suggests an optimised design sizing of the rotor to manage relative velocities and reduce aerodynamic loading on rotor blades. Managing the relative Mach number minimises velocity losses and improves energy conversion efficiency. Maintaining balanced relative Mach numbers ensures optimal aerodynamic and structural performance limits for the turbine [29]. Finally, the physical characteristics of the turbine can be identified from the analysis conducted in Figures 7 to 11. Table 2 shows the design specifications. The flow at the exit of the turbine was set to be axial; thus, the $\alpha_2 = 0$. The number of blades was obtained using Eq. (5), and the number of blades for the turbine is 11. The thickness of the blade is 1.0 mm, and the blockage factor, *B*, is 20%.

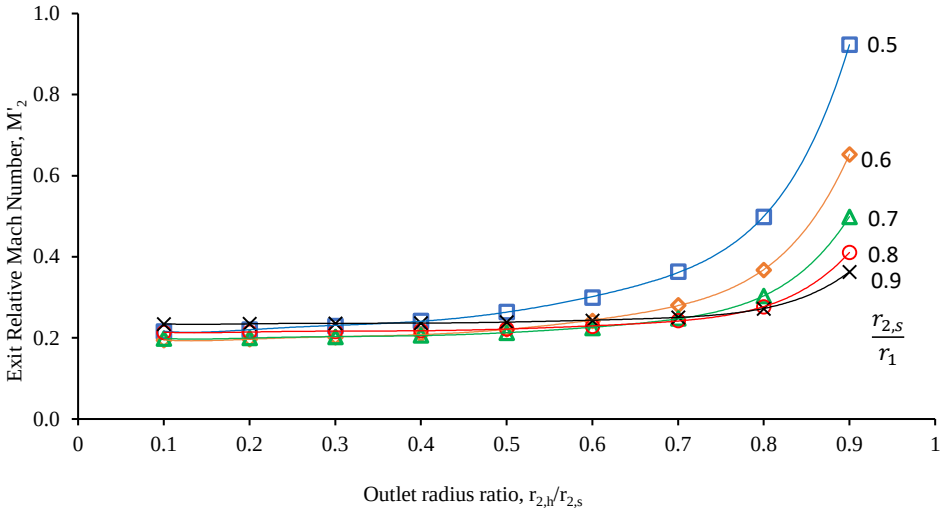

Figure 11. Exit relative Mach number, M'_2 at various $r_{2,h}/r_{2,s}$

Table 2. Results of turbine design parameters

Items	Specifications
Inlet radius, r_1 (mm)	19.3
Length of leading edge (mm)	4.5
Inlet absolute angle, α_1 (°)	72
Exit radius ratio, $r_{2,h}/r_{2,s}$	0.7
Exit relative angle, β_2 (°)	-61
Number of blades	11
Thickness of blades (mm)	1
Blockage factor, B (%)	20

Figure 12(a) shows the camberline of a rotor for a radial turbine. Camberline is one of the important parameters of blade design, which means line along the blade from the leading edge to the trailing edge. The camber line graph shows the curvature profile of the blade along its length. The curve starts from the origin as the blade's leading edge, with a constantly increasing slope indicating the degree of curvature of the blade. The steep slope indicates the high camber towards the rear edge to ensure proper airflow through the turbine. This camber line design is critical for improving the aerodynamics of the turbine blade, minimising flow separation, and raising efficiency [10]. Figure 12(b) shows a rotor's meridional section. The curvatures were generated by using the Bezier polynomials equations, which are widely used in aerodynamic design and will produce smooth curves. This was employed to define the geometry of the rotor blade in different sections. The outermost curve refers to the hub section of the rotor and goes to the shroud. A meridional section graph using Bezier curves helps outline the blade to maintain a smooth flow.

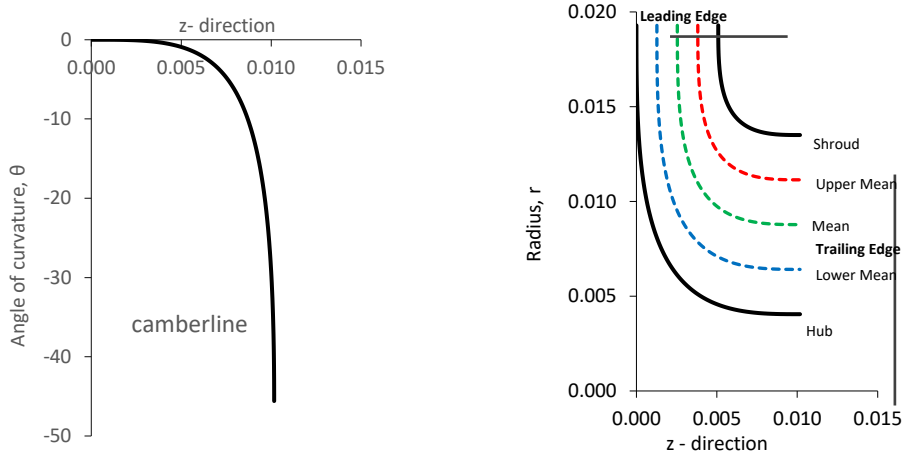

(a) (b)

Figures 12. Curvature for the turbine rotor: (a) Camberline and (b) Meridional

3D geometry involves representing objects or shapes within a three-dimensional area. In contrast to 2D geometry, which focuses on flat shapes, 3D geometry includes depth, width, and height to create a more realistic depiction of objects.

The use of CATIA for geometric design is often compared to other software tools. For example, integrating CATIA with MS Excel and Autodesk Inventor can enhance the overall design workflow, providing a comprehensive solution for creating detailed and complex geometries. This synergy is particularly advantageous for optimising design parameters and improving the manufacturability of turbine components [30]. The basic geometric layout of the radial turbine rotor was defined. The outline was developed using initial calculations and design principles. The blade profile stood out as the important element of the rotor configuration. Following the initial establishment of the outline structure, a detailed design was done to enhance the geometry. This involved utilising CATIA's surface modelling tools; seamless surfaces were generated for blades for each part. The turbine blades' distribution is shown in Figure 13 and how they are positioned around the rotor hub. This condition was commonly observed in radial turbines where the blades were positioned relative to each other from a central point to allow the fluid to pass through in a radial flow through the turbine. The arrangement ensured that flow was distributed evenly and increased the turbine's performance. The 3D geometric configuration of a radial turbine rotor was developed and constructed. This emphasised capturing the detail of blade profiles. The turbine's rotor was drawn in every detail to ensure the viewer understood how the device worked and its main components. During the modelling process, three-dimensional computer-aided design software was used to create the turbine. The final model of the radial turbine rotor is a 3D model. Moreover, it emphasised the significance of the accurate geometric design of blades in radial turbines and paved the way for further innovations and developments.

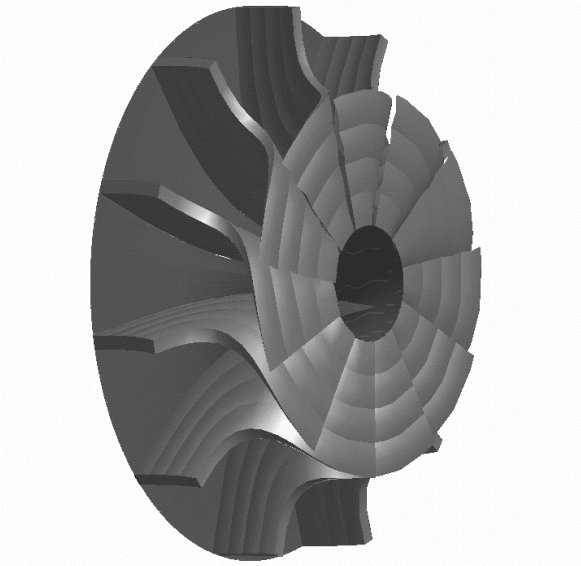

Figure 13. 3D model of the turbine rotor

3.2 Computational Performance

The performance map in Figure 14 shows how a radial turbine's Mass Flow Parameter (MFP) changes with Pressure Ratio (PR) at different rotational speeds (50,000 RPM, 70,000 RPM, and 90,000 RPM). The map trend is a common trend that was published by Whitfield [11]. As PR increases, MFP rises for all speeds, but the increase is more pronounced at lower PRs. At 50,000 RPM, the turbine can handle the highest mass flow, making it the most efficient speed. However, as the RPM increases to 70,000 and 90,000, the radial turbine's ability to handle mass flow decreases, likely due to increased aerodynamic and mechanical losses. The performance map also hints at the phenomenon of choking. Choking occurs when the turbine reaches a point where increasing the PR further does not result in a higher mass flow, as the flow speed reaches the speed of sound; consequently, the exit relative velocity discharge is greater than the inlet. Figure 14 indicates this by the flattening of the curves at higher PRs, particularly at higher RPMs like 90,000 RPM. The designed turbine is choked approximately at PR≈1.4, it is observed. At this point, the turbine cannot pass more mass flow, regardless of further increases in PR, signalling the onset of choking. The flow limitation has reduced the turbine's performance, as the efficiency drops and the turbine can no longer increase its output.

Figure 15 shows the Total-to-Static Efficiency, η_{T-s} of a radial turbine as a function of the Velocity Ratio, U_2/C_{is} for three different rotational speeds; 50,000 RPM, 70,000 RPM, and 90,000 RPM. The efficiency increases with the velocity ratio, reaches a peak, and then declines, forming a parabolic curve for each speed. The highest efficiency is achieved at 70,000 RPM, peaking around 67% at a velocity ratio near 0.4. For 50,000 RPM, the peak efficiency is slightly lower, around 55%, while at 90,000 RPM, the maximum efficiency is about 60% at a higher velocity ratio. These observations highlight the optimal operating point for each speed, where the turbine performs most efficiently in converting kinetic energy into useful work. The efficiency trends observed in the graph are significantly influenced by aerothermodynamic effects, which encompass the interactions between thermal and aerodynamic processes within the turbine [28]. As the bulk air increases, the relative velocity of the working fluid also increases, leading to changes in the turbine's temperature, pressure, and velocity fields. These changes affect the thermodynamic cycle and aerodynamic losses, influencing the overall efficiency.

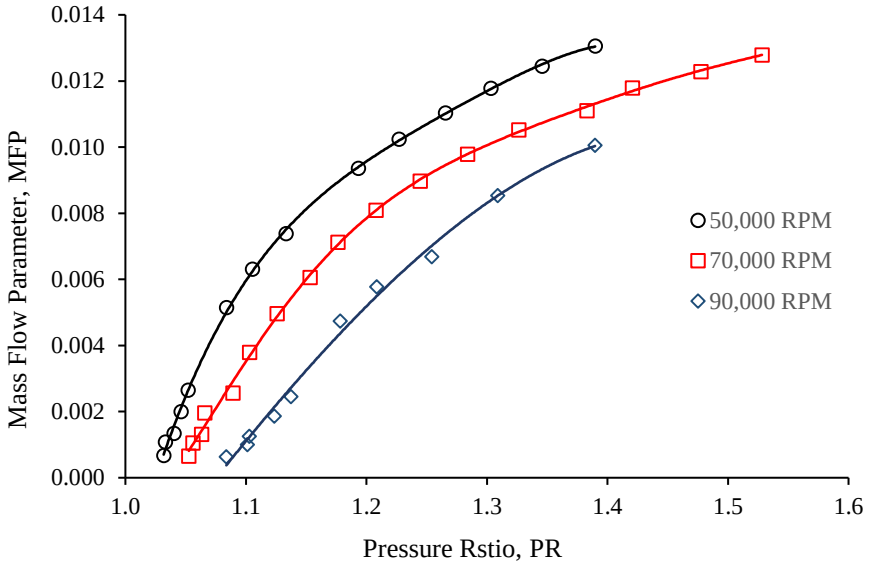

Figure 14. Pressure ratio versus mass flow parameter

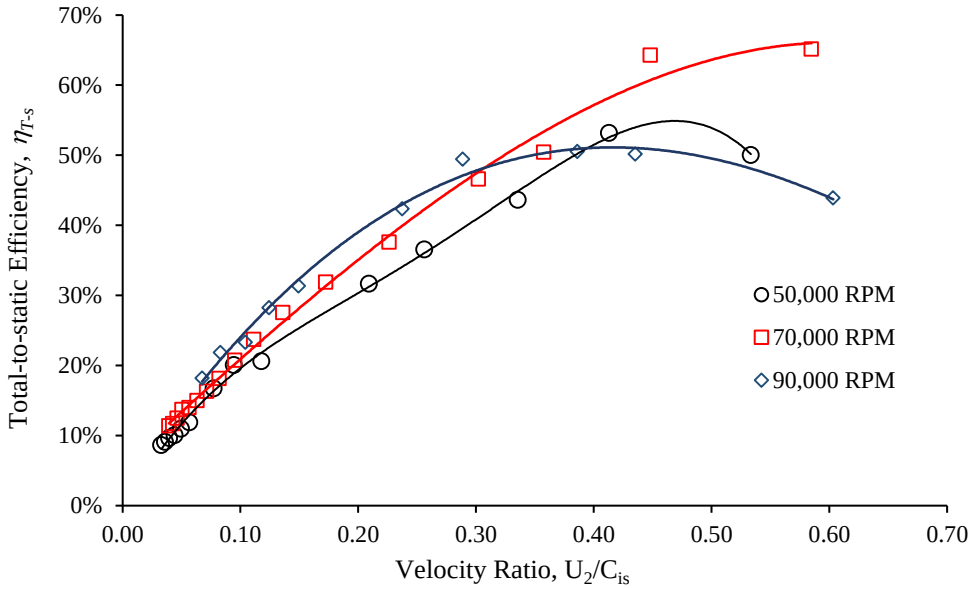

Figure 15. Total-to-static efficiency at various turbine speed

At higher rotational speeds, such as 90,000 RPM, the increased velocity of the working fluid raises the total temperature, leading to higher heat losses through conduction, convection, and radiation. This temperature rise can affect the fluid's properties, such as density and viscosity, leading to higher aerodynamic losses, including increased friction and flow separation (secondary flow and vorticity). The compressibility effects become more pronounced at these higher speeds, contributing to shock losses and further reducing efficiency after the peak velocity ratio is reached. These losses are reflected in the sharper decline in efficiency observed at 90,000 RPM compared to lower speeds.

The absolute angle, α and incidence angle, *i*, at the turbine inlet are crucial factors in determining the turbine's performance. The optimum range for *i* is -20≤ I ≤-40, according to Japikse [31]. The α is the angle at which the flow enters the turbine blades relative to the axial direction, while the incidence angle is the angle between the incoming flow and the blade's leading edge. Both angles significantly impact the efficiency by influencing the aerodynamic loading on the blades and the flow behaviour within the turbine [29]. At lower velocity ratios, where the flow velocities are relatively low, the incidence angle tends to be small, leading to favourable flow conditions with minimal flow separation and lower aerodynamic losses. This condition is generally associated with higher efficiencies, as seen in the graph's initial increase in efficiency. However, as the velocity ratio increases, the flow velocity at the turbine inlet also increases, which can result in a higher incidence angle. A large incidence angle can cause the flow to deviate significantly from the blade's surface, leading to flow separation and increased pressure losses. These aerodynamic losses are reflected in the decreased efficiency observed beyond the peak velocity ratio for each rotational speed.

The α also plays a critical role in determining the turbine's performance. In the radial turbine, the α is determined by the volute cross-sectional area [8]. If the absolute angle is not optimised for a given rotational speed, the flow can enter

the turbine blades at too steep or shallow angle, leading to suboptimal flow conditions. A steep absolute angle can result in excessive aerodynamic loading on the blades, causing increased frictional losses and potential blade vibration or fatigue. On the other hand, a shallow absolute angle can lead to insufficient aerodynamic loading, reducing the turbine's ability to extract energy from the fluid effectively. In Figure 16, the differences in peak efficiency at various rotational speeds can be partially attributed to variations in the absolute and incidence angles at the turbine inlet. At 70,000 RPM, the turbine likely operates with an optimal combination of absolute and incidence angles, leading to the highest efficiency. At 50,000 RPM and 90,000 RPM, the deviation from these optimal angles could result in higher aerodynamic losses and lower peak efficiencies.

3.3 Rotor Aerodynamic Flow Field

Understanding the rotor aerodynamic flow field in the CFD analysis requires a detailed examination of physical properties like pressure, static entropy, and velocity within a fixed frame of reference. Velocity, which refers to the speed and direction of fluid flow from a fixed point in space, is crucial for comprehending how fluid moves through rotor blades. By analysing velocity vectors and magnitudes, one can identify wake zones where velocity decreases due to flow separation or energy extraction, which is critical in optimising blade design. Variations in fluid velocity as it interacts with each blade can reveal areas where energy conversion is particularly efficient, as indicated by elevated speeds in the stationary frame. This understanding allows engineers to pinpoint regions where blade design can be improved to reduce aerodynamic losses and increase efficiency, contributing to the overall performance of the turbine.

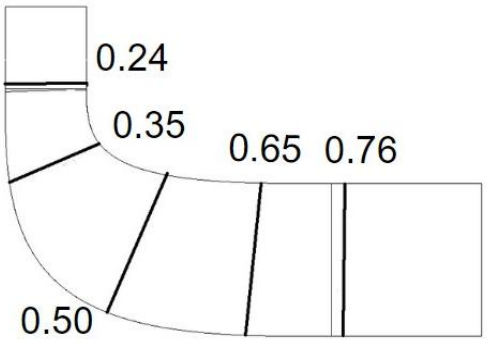

Figure 16. Spanwise cross-section location

Static entropy, which measures the disorder of fluid molecules, is another vital parameter in assessing energy conversion efficiency in a turbine. Lower entropy changes across the rotor blades indicate more effective energy conversion, whereas high entropy regions suggest energy losses due to shock waves, turbulence, or friction. By understanding entropy changes, engineers can better evaluate the thermodynamic efficiency of the turbine and identify areas where performance improvements can be made. Additionally, pressure, the force exerted by the fluid per unit area in the stationary frame, is essential for determining blade loading and identifying significant pressure drops. These drops indicate the conversion of pressure energy into mechanical work, which is crucial for efficient energy extraction. The effect of the entropy generated is depicted in Figure 2, where the entropy generated has decreased the energy output from the gas expansion process in the turbine. The static entropy contour can be visualised in the turbine passage. Figure 16 shows a cross-sectional view of a turbine blade, with specific measurements at various segments (0.76, 0.65, 0.50, 0.35, 0.24) along its spanwise direction. These measurements, extending from the root to the tip, are essential for evaluating the turbine's structural integrity, power output, and efficiency. By summing the segment measurements, one can determine the overall span size of the blade, which plays a crucial role in the blade's aerodynamic performance.

Figure 17 shows the flow field analysis at various cross-sections in the spanwise direction of the turbine. The analysis was done at the design point, where the mass flow rate is 0.025 kg/s, and the rotational speed is 70,000 RPM. The performance analysis of a high-pressure turbine provides essential insights into the thermodynamic and mechanical processes that govern the expansion process in the turbine. One of the key indicators of performance is the change in the working fluid's total enthalpy, which decreases from 504,757 J/kg at the turbine's intake to 511,681 J/kg at the outflow. This reduction in enthalpy reflects the turbine's ability to extract energy from the fluid, most of which is converted into mechanical shaft work that drives electrical generators or subsequent turbine stages. Alongside the enthalpy drop, the fluid's pressure decreases from 117,120 Pa to 109,018 Pa, generating the force necessary to rotate the turbine blades and shaft.

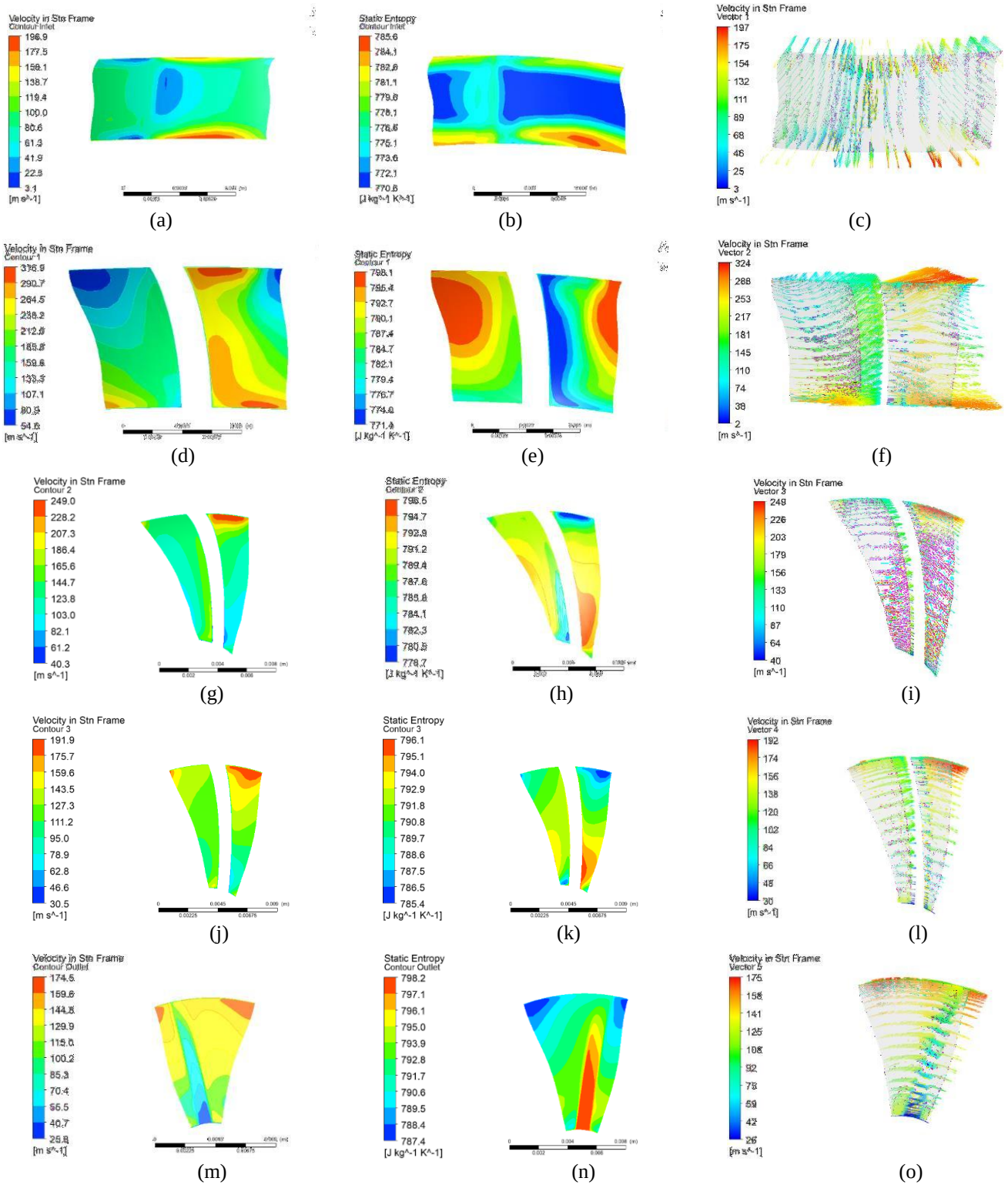

Figure 17. The absolute velocity, static Entropy and velocity vector analysis in various cross section: (a-c) 0.24 span, (d-f) 0.35 span, (g-i) 0.5 span, (j-l) 0.65 span and (m-o) 0.76 span

The fluid's velocity also changes significantly, increasing from 61.5 m/s at the intake to 129.7 m/s at the outflow. This fluid acceleration is crucial for converting pressure energy into kinetic energy, demonstrating the turbine's efficiency in producing mechanical energy. The interplay between fluid dynamics and thermodynamics is further evidenced by the variation in velocity and its impact on static entropy across different turbine blade sections. The analysis of flow vorticity, particularly its effect on static entropy, reveals how aerodynamic forces and flow patterns influence energy conversion efficiency [18]. The velocity is relatively low at the root section (0.24 span) due to reduced aerodynamic interaction, resulting in steady flow conditions and higher total pressure. The static entropy at this span is also low, indicating effective energy transmission with minimal turbulence and irreversibility. The $\eta_{T-s}$is quantified by the amount of entropy generated in the fluid flow passage. The higher the entropy generated, the lower will be the η_{T-s}. Therefore, the blade

profile of the radial turbine must be optimised to reduce the aerodynamic interaction that will control the velocity gradient in the flow passage. A higher velocity gradient will contribute to the higher entropy generated in the flow passage.

The passage velocity increases as the flow progresses toward the mid-span (0.35 to 0.50 span), leading to higher aerodynamic forces and more complex flow patterns. A more complex flow pattern gradually increases static entropy, signifying rising irreversibility and energy loss due to turbulence. By the mid-span, the blade experiences significant aerodynamic loading, further accelerating the fluid and increasing entropy. This mid-span region is characterised by notable energy dissipation, as evidenced by the continued drop in total pressure and the rise in static entropy. The aerodynamic forces become more pronounced, contributing to greater flow turbulence and energy conversion losses. Approaching the tip from 0.65 to 0.76 span, the velocity reaches its maximum, leading to the most significant aerodynamic interactions and the highest levels of static entropy. The blade encounters the strongest aerodynamic forces at these spans, resulting in substantial energy dissipation and the lowest total pressure. The elevated static entropy near the tip reflects high turbulence and irreversibility, corresponding to the greatest inefficiency in energy conversion along the blade span. This analysis highlights the critical role of flow vorticity and its influence on static entropy in determining the overall efficiency of the high-pressure turbine, with the most significant inefficiencies occurring near the blade tip due to complex aerodynamic phenomena.

4. CONCLUSION

This paper presents a comprehensive numerical analysis and design optimisation of a 500W high-pressure radial turbine to effectively harness exhaust energy from an internal combustion engine. The turbine's physical dimensions were meticulously optimised by employing fundamental thermodynamic principles and Euler turbomachinery equations, including an inlet radius of 19.3 mm, an inlet absolute angle of 72°, and an outlet radius ratio of 0.7. The CFD simulations conducted at varying rotational speeds (50,000, 70,000, and 90,000 RPM) revealed critical insights into the turbine's performance, with a peak total-to-static efficiency of 67% observed at 70,000 RPM. The paper's findings emphasise the significance of precise geometric and aerodynamic optimisation in achieving high efficiency in radial turbines. The flow field analysis further highlighted the importance of managing velocity gradients and static entropy within the rotor passage to minimise energy losses and maximise performance. This research offers valuable contributions to developing high-performance radial turbines, particularly in applications where efficient energy recovery is paramount.

ACKNOWLEDGMENTS

This study was not supported by any grants from funding bodies in the public, private, or not-for-profit sectors.

CONFLICT OF INTEREST

The authors declare no conflicts of interest.

AUTHORS CONTRIBUTION

N. S. Ahmad (Methodology; Data curation; Formal analysis; Visualisation; Writing - original draft)

M. N. Azman (Methodology; Data curation; Software; Formal analysis; Writing - original draft)

A. M. I. Bin Mamat (Conceptualisation, Validation; Formal analysis; Writing - review & editing; Supervision)

AVAILABILITY OF DATA AND MATERIALS

The data supporting this study’s findings are available on request from the corresponding author.

ETHICS STATEMENT

Not applicable

REFERENCES

[1] A. F. Yusop, R. Mamat, M. H. Mat Yasin, O. M. Ali, “Effects of particulate matter emissions of diesel engine using diesel-methanol blends,” *Journal of Mechanical Engineering and Sciences*, vol. 6, no. 2, pp. 959–967, 2014.

[2] N. R. Abdullah, N. S. Shahruddin, R. Mamat, A. M. I. Mamat, A. Zulkifli, “Effects of air intake pressure on the engine performance, fuel economy and exhaust emissions of a small gasoline engine,” *Journal of Mechanical Engineering and Sciences*, vol. 6, no. 2, pp. 959–968, 2014.

[3] N. Watson, M. S. Janota. Turbocharging the Internal Combustion Engine. 1st Ed. London: The McMillan Press Ltd, 1982.

[4] M. Ingale, H. Kawale, A. Thakre, N. Shrikhande, “Performance enhancement of engine using turbocharger-A review,” *International Journal of Creative Research Thoughts*, vol. 6, no. 1, pp. 6–10, 2018.

[5] H. Chen, N. C. Baines, "Analytical optimization design of radial and mixed flow turbines," *Proceedings of the Institution of Mechanical Engineers, Part A: Journal of Power and Energy*, vol. 206, no. 3, pp. 177–187, 1992.

[6] A. M. I. B. Mamat, R. F. Martinez-Botas, "Mean line flow model of steady and pulsating flow of a mixed-flow turbine turbocharger," in *Proceedings of the ASME Turbo Expo*, vol. 7, no. 246, pp. 2393–2404, 2010.

[7] R. S. R. Gorla, A. A. Khan. Chapter 7: Axial Flow and Radial Flow Gas Turbines in Turbomachinery Design and Theory. 1st Ed. Boca Raton: CRC Press, 2021.

[8] C. Li, H. Chen, Y. Wang, Y. Wei, G. Wu, "An investigation of the effects of volute A/R distribution on radial turbine performance," *Proceedings of the Institution of Mechanical Engineers, Part D: Journal of Automobile Engineering*, vol. 238, pp. 3242–3252, 2023.

[9] C. Li, Y. Wang, X. Li, H. Chen, Y. Wei, G. Wu, "A two-dimensional method for radial turbine volute design," *Proceedings of the Institution of Mechanical Engineers, Part A: Journal of Power and Energy*, vol. 237, no. 1, pp. 33–47, 2023.

[10] L. Jun, X. Jinli, J. Rui, W. Hanbin, "Design and analysis of radial turbine rotor based on Bezier curve method," *International Journal of Research in Mechanical Engineering*, vol. 3, no. 5, pp. 49–54, 2015.

[11] A. Whitfield, "The preliminary design of radial inflow turbines," *Journal of Turbomachinery*, vol. 112, no. 1, pp. 50–57, 1990.

[12] A. M. I. Bin Mamat, R. F. Martinez-Botas, S. Rajoo, L. Hao, A. Romagnoli, "Design methodology of a low pressure turbine for waste heat recovery via electric turbocompounding," *Applied Thermal Engineering*, vol. 107, no. 4, pp. 1166–1182, Aug. 2016.

[13] A. K. Noughabi, S. Sammak, "Detailed design and aerodynamic performance analysis of a radial-inflow turbine," *Applied Sciences (Switzerland)*, vol. 10, no. 11, pp. 1–15, 2018.

[14] A. A. Ahmad Zahidin, A. M. I. Mamat, A. Romagnoli, "Computational performance of a-100 kW low pressure turbine to recover gas turbine exhaust energy," *Journal of Mechanical Engineering and Sciences*, vol. 13, no. 2, pp. 4777–4793, 2019.

[15] Z. Zulkifli, N. H. Abdul Halim, Z. H. Solihin, J. Saedon, A. A. Ahmad, A. H. Abdullah, et al., "The analysis of grid independence study in continuous disperse of MQL delivery system," *Journal of Mechanical Engineering and Sciences*, vol. 17, no. 3, pp. 9586–9596, 2023.

[16] E. Septyaningrum, R. Hantoro, I. K. A. P. Utama, J. Prananda, G. Nugroho, A. W. Mahmashani, et al., "Performance analysis of multi-row vertical axis hydrokinetic turbine-straight blade cascaded (VAHT-SBC) turbines array," *Journal of Mechanical Engineering and Sciences*, vol. 13, no. 3, pp. 5665–5688, 2019.

[17] B. Ahmad, A. Fattah, A. M. I. Bin Mamat, "Single passage CFD analysis for non-radial fibre element of low pressure turbine," *Jurnal Teknologi*, vol. 76, no. 5, pp. 67–72, 2015.

[18] A. Borovkov, I. Voinov, Y. Galerkin, R. Kamin, A. Drozdov, O. Solovyeva, et al., "Design, plant test and CFD calculation of a turbocharger for a low-speed engine," *Applied Sciences (Switzerland)*, vol. 10, no. 23, pp. 8344–8352, 2020.

[19] X. Yu, M. Li, G. An, B. Liu, "A coupled effect model of two-position local geometric deviations on subsonic blade aerodynamic performance," *Applied Sciences (Switzerland)*, vol. 10, no. 24, pp. 8976–8985, 2020.

[20] K. I. Hamada, M. M. Rahman, D. Ramasamy, M. M. Noor, K. Kadirgama, "Numerical investigation of in-cylinder flow characteristics of hydrogen-fuelled internal combustion engine," *Journal of Mechanical Engineering and Sciences*, vol. 10, no. 1, pp. 1792–1802, 2016.

[21] M. P. Helios, W. Asvapoositkul, "Numerical studies for effect of geometrical parameters on water jet pump performance via entropy generation analysis," *Journal of Mechanical Engineering and Sciences*, vol. 15, no. 3, pp. 8319–8331, 2023.

[22] N. N. Bayomi, "Radial turbine design process," *Journal of Science and Technology*, vol. 11, no. 19, pp. 9–22, 2015.

[23] A. F. El-Sayed. Aircraft Propulsion and Gas Turbine Engines. 1st Ed. Boca Raton: CRC Press, 2017.

[24] E. Sauret, "Open design of high pressure ratio radial-inflow turbine for academic validation," *ASME International Mechanical Engineering Congress and Exposition, Proceedings (IMECE)*, vol. 7, no. 1, pp. 3183–3197, 2012.

[25] B. E. Launder, D. B. Spalding, "The numerical computation of turbulent flows," *Computer Methods in Applied Mechanics and Engineering*, vol. 3, no. 2, pp. 269–289, 1974.

[26] M. Tancrez, J. Galindo, C. Guardiola, P. Fajardo, O. Varnier, "Turbine adapted maps for turbocharger engine matching," *Experimental Thermal and Fluid Science*, vol. 35, no. 1, pp. 146–153, 2011.

[27] A. Mobarak, M. G. Khalafallah, A. M. Osman, H. A. Heikal, "Experimental investigation of secondary flow and mixing downstream of straight turbine cascades," Journal of Turbomachinery, vol. 110, no. 4, pp. 497–503, 1988.

[28] A. Meroni, M. Robertson, R. Martinez-Botas, F. Haglind, "A methodology for the preliminary design and performance prediction of high-pressure ratio radial-inflow turbines," *Energy*, vol. 164, pp. 1062–1078, 2018.

[29] A. Leto, "Radial turbine preliminary design and performance prediction," in *AIP Conference Proceedings*, vol. 2191, no. 1, pp. 1–9, 2019.

[30] G. N. Koini, S. S. Sarakinos, I. K. Nikolos, "A software tool for parametric design of turbomachinery blades," *Advances in Engineering Software*, vol. 40, no. 1, pp. 41–51, 2009.

[31] D. Japikse, N. C. Baines. Introduction to Turbomachinery. 1st Ed. United States: Concepts ETI, 1994.